Combining nano-silicon with oxide glass in anodes for Li-ion batteries

Yan, Jiajia; Zheng, K.; Shi, N.; Ren, X.L.; Zhou, H.M.; Tao, H.Z.; Ren, J.J.; Qiao, A.; Zhang, Y.F.; Yue, Yuanzheng

Published in:
Journal of Non-Crystalline Solids

DOI (link to publication from Publisher):
10.1016/j.jnoncrysol.2024.122964

Publication date:
2024

Document Version
Publisher's PDF, also known as Version of record

Journal of Non-Crystalline Solids 633 (2024) 122964

Contents lists available at ScienceDirect

Journal of Non-Crystalline Solids

journal homepage: www.elsevier.com/locate/jnoncrysol

Combining nano-silicon with oxide glass in anodes for Li-ion batteries

Jiajia Yan [a], Kai Zheng [b], Nian Shi [c], Xianglong Ren [d], Hemin Zhou [d], Haizheng Tao [d], Jinjun Ren [c], Ang Qiao [d], Yanfei Zhang [b,*], Yuanzheng Yue [a,*]

[a] Department of Chemistry and Bioscience, Aalborg University, 9220 Aalborg, Denmark
[b] School of Materials Science and Engineering, Qilu University of Technology, Jinan 250353, PR China
[c] Key Laboratory of Materials for High Power Laser, Shanghai Institute of Optics and Fine Mechanics, Chinese Academy of Sciences, Shanghai 201800, PR China
[d] State Key Laboratory of Silicate Materials for Architectures, Wuhan University of Technology, Wuhan 430070, PR China

ARTICLE INFO

Keywords:
Vanadium-tellurite glass
Silicon (Si)
Si@glass composite
Anode
Lithium-ion batteries

ABSTRACT

Vanadium-tellurite glasses (VT) have emerged as promising anode materials for lithium-ion batteries (LIBs). Despite this, the Li-ion storage capacity of the VT glass anode is still insufficient to meet the demands for the next generation of advanced LIBs. Silicon (Si) anode has ultrahigh theoretical capacity but suffers from significant volume expansion during lithiation and delithiation. In this work, we combined Si nanoparticles with VT glass to prepare Si@VT composite anode for LIBs. The composite was produced through heat-treatment at different temperatures, some of which were hot-pressed under the isostatic pressure of 100 MPa. The Si@VT composite exhibited a synergistic effect that integrated the strengths of both VT glass and Si, resulting in a substantial enhancement of its electrochemical performance. The systematic characterizations of the composite-based anodes revealed the optimal conditions for fabricating the high-performance Si@VT composite: a silicon fraction of 10 wt% and a hot-pressing temperature of 620 K. This composite stood out as the optimal choice, exhibiting a capacity of 353 mA h g^{-1} at 1 A g^{-1} after 1000 cycles. This capacity surpasses that of VT glass anode by over threefold and that of pure Si anode by twelvefold.

1. Introduction

With the merits of high energy density, long lifespan, and environmental friendliness, lithium-ion batteries (LIBs) represent one of the most attractive portable energy storage devices. However, the current LIBs cannot satisfy the demands for safer and higher energy density batteries used in electric vehicles and large-scale energy storages [1]. To tackle these problems, many efforts have been made. In the pursuit of enhanced safety, all-solid-state batteries have attracted considerable attention and extensive research. They represent a change from conventional organic liquid electrolytes to solid electrolytes, with inorganic glass or glass-ceramic based solid electrolytes as highly promising candidates owing to their high ionic conductivities, typically ranging from 10^{-2} to 10^{-3} S cm^{-1} [2–5]. To achieve high energy density (proportional to specific capacity) in LIBs, a crucial strategy is to substitute silicon (Si) for the commercial graphite in anodes. Silicon exhibits an ultrahigh theoretical capacity, surpassing 4000 mA h g^{-1}, more than 11 times the capacity of the commercial graphite [1,6]. Nonetheless, the drastic volume fluctuation of Si (~400%) during lithiation/de-lithiation [1] leads to a dramatic decay of specific capacity, i.e., the capacity remains only about 50 mA h g^{-1} within 100 cycles [7,8]. To counteract the volume expansion of Si, various structures, including hollow core-shell, york-shell, porous configurations, in combination with carbon, were created [9–13]. These structures were predominantly constructed using the sol-gel method, solvothermal method, chemical vapor deposition, among others. However, the practical applications of these structures are limited owing to their complex synthesis processes, low yield and high cost [2].

Vanadium-tellurite (VT) glass-based anodes for LIBs exhibit a superior cycling stability, i.e., almost no capacity fading after 5000 cycles [14,15]. Their high cycling stability was attributed to both the open network structure and strong crystallization tendency of VT glasses. During discharging/charging process, electrochemically active γ-Li_3VO_4 nanocrystals form in VT glasses. The nanocrystals not only toughen the glass matrix, thereby increasing the cycling stability, but also provide more space/channels between the crystals and glass matrix to facilitate the transfer kinetics of Li^+ ions [14–20]. However, despite exhibiting excellent cycling stability, VT glass anodes still have relatively low

* Corresponding authors.
E-mail addresses: zhang-yanfei@hotmail.com (Y. Zhang), yy@bio.aau.dk (Y. Yue).

https://doi.org/10.1016/j.jnoncrysol.2024.122964
Received 26 January 2024; Received in revised form 14 March 2024; Accepted 4 April 2024

capacity, typically around 120 mA h g^{-1} at a current density of 1 A g^{-1} [14,15]. Therefore, there is a need for further enhancement. Hence, we anticipate that combing Si with VT glass could be a promising strategy to achieve the synergetic effect, enhancing both the capacity and cycling stability of the anode for LIBs. Furthermore, all-solid-state LIBs encounter a significant challenge regarding the interfacial stability between the glassy solid-state electrolyte and the conventional electrode, stemming from their poor compatibility [4]. It is anticipated that the composite comprising Si and VT glass (referred to as Si@VT composite) would demonstrate robust compatibility with the glassy/glass-ceramic electrolytes. This is attributed to the shared presence of the glass phase in both the electrolytes and VT anodes. This compatibility might effectively reduce the interfacial polarization within the cell. Additionally, glass materials pose many other advantages, e.g., tunable composition, simple preparation process, and low cost. Therefore, it is a promising way to incorporate high-capacity elements, e.g., Si, into glasses matrix for developing the next generation of high-performance LIBs, in particular, all-solid-state LIBs.

Recently, we have investigated how Si-doping affects the structure and crystallization behavior of VT glasses during heating process [16]. Using the previous findings as guide, in this work, we synthesized a series of composite containing both Si and VT glass (Si@VT) in different ratio. Some of these composites were subjected to heat treatment at various temperatures above the glass transition temperature (T_g) under different pressure (0 and 100 MPa). During heat-treatment, the VT glass acted as 'binder' through its viscous flow to bond with Si. Then, the electrochemical performances of the derived Si@VT composites were systematically investigated. It is found that the Si@VT composite after hot pressing exhibited a reversible specific capacity of 353 mA h g^{-1} at 1 A g^{-1} after 1000 cycles, which is more than three times that of VT glass anode and twelve times that of pure Si anode under the same testing condition. This work not only introduced an optimized strategy for fabricating Si@VT composites, enhancing their performance as anodes for LIBs through hot-pressing technique, but also paved a new path for developing glass-based functional materials.

2. Experimental section

2.1. sample preparation

The $50V_2O_5$–$50TeO_2$ (in mol%) (VT) glass was prepared via melt-quenching [14,15]. Afterwards, it was crushed to glass powders with sizes ranging approximately from 10 to 20 μm. Commercial nano-silicon powder in quantities of 0.1, 0.2, 0.3, and 0.4 g (with particle size of about 20–60 nm) were individually mixed with 0.9, 0.8, 0.7, and 0.6 g of glass powders, respectively. These mixtures denoted as 10SiVT, 20SiVT, 30SiVT, 40SiVT, according to the weight fraction of Si. The V_2O_5, TeO_2, and commercial nano-silicon powders used in this study were purchased from Shanghai Aladdin Bio-Chem Technology Co., LTD. To find out a proper hot-pressing condition, 10SiVT glass was hot-pressed at different temperatures in a vacuum furnace under 100 MPa and kept for 0.5 h. The selection of the heat-treatment temperatures was based on the characteristic temperatures of the samples, determined during heating to 773 K at a rate of 10 K/min in an argon atmosphere using a differential scanning calorimeter (DSC) (Fig. S1). The characteristic temperatures include the glass transition temperature T_g (509 K), the first and second crystallization onset temperatures T_{c1} and T_{c2} (563 and 602 K, respectively), and the melting temperature T_m (755 K). Specifically, 10SiVT was hot-pressed at 550 K (above T_g), 570 K (above T_{c1}), 620 K (above T_{c2}), 670 K (below T_m), and 770 K (above T_m), respectively. The resulting samples are denoted as 10SiVT-550-P, 10SiVT-570-P, 10SiVT-620-P, 10SiVT-670-P, and 10SiVT-770-P, respectively, according to the hot-pressing temperature. For comparison, 10SiVT was heated to 620 K and kept for 0.5 h in the vacuum furnace without pressure, and then naturally cooled down to room temperature. The obtained sample is named as 10SiVT-620. Furthermore, to find the optimal fraction of Si for achieving the superior composite anodes, additional samples, such as 20SiVT-620-P, 30SiVT-620-P, 40SiVT-620-P, were also prepared.

2.2. Material characterization

The crystal phases of samples after heat-treatment were identified on a PANalytical X-ray diffractometer with Cu Kα (λ = 1.5406 Å) radiation during the 2θ range of 5∼70° with a step size of 0.013° The characteristic temperatures of the samples were identified by a DSC (Jupiter 449C, Netzsch) under the above-mentioned conditions (Section 2.1). Fourier transform infrared (FTIR) spectra were obtained on a Bruker TENSOR II FTIR spectrometer with Platinum ATR Accessory at room temperature in the range of 400–4000 cm^{-1}. To study the chemical environment of V and Si, X-ray photoelectron spectroscopy (XPS) was performed using ESCALAB 250Xi spectrometer (ThermoFisher Scientific, USA) with nonmonochromatic Al Ka X-ray (1486.6 eV) at pass energy of 50 eV. The morphologies and distribution of Si in samples were analyzed using field-emission scanning electron microscopy (FE-SEM) (Supra-55, Zeiss Inc.), and X-ray energy dispersive spectroscopy (EDS) (X-Max, OXFORD Instruments Inc.).

2.3. Cell assembly and electrochemical characterization

The electrochemical performance of Si@VT composite after heat-treatment was evaluated using CR2032 coin cells with lithium foil as the reference electrode. The Si@VT (70 wt%), acetylene black (20 wt%), and polyvinylidene difluorides (PVDF, 10 wt%) were mixed evenly in N-methyl-2-pyrrolidone (NMP) and then pasted onto a copper foil substrate and dried at 110 °C in a vacuum oven for 12 h to get working electrodes. 1 M $LiPF_6$ in ethylene carbonate (EC)/diethyl carbonate (DEC)/dimethyl carbonate (DMC) (1:1:1 vol%) was used as the electrolyte and the Celgard 2325 membrane (diameter of 19.0 mm) was used as the separator. Cells were assembled in an argon-filled glovebox with both the moisture and the oxygen content below 0.1 ppm and then tested at 298 K. The galvanostatic charging/discharging tests of the samples were conducted on a Land battery test system (CT2001A) with the voltage range of 0.01–3 V. Cyclic voltammetry (CV) curves were obtained in the voltage range of 0.01–3 V at the scanning rate of 0.1 mV s^{-1}. EIS spectra were recorded in the frequency range of 0.1–100 kHz on CHI 760e electrochemical workstation. All electrochemical measurements were repeated with different batches of samples to confirm the reproducibility of their performances.

3. Results and discussion

3.1. The phase and microstructure of the as-received Si@VT composite

Fig. 1 shows the XRD patterns of 10SiVT hot-pressed at different temperatures. It is seen that three sharp diffraction peaks appear at 28°, 47°, 56° of 2θ, respectively, for the five samples. The peaks are ascribed to Si, indicating that Si is preserved in the composite after heat-treatment. In addition, additional V_2O_5 and $TeVO_4$ crystals can be observed in 10SiVT-670-P and 10SiVT-770-P samples. However, despite heat-treating 10SiVT-570-P and 10SiVT-620-P at temperatures above the first crystallization onset temperature T_{c1} (563 K), as shown in Fig. S1, no detectable new crystals were formed in both samples. Absence of crystal formation could be due to the sample temperature being lower than the temperature indicated on the heating furnace. In contrast, the temperature indicated on the DSC matches the sample temperature accurately, as the thermal couples of the DSC are directly linked to the platinum crucible containing the samples.

To study the effect of hot-pressing process on the phase transitions in the samples, we performed DSC measurements on both 10SiVT and 10SiVT-620-P. Fig. 2 shows the first DSC upscan curves of 10SiVT and 10SiVT-620-P, obtained by heating to 773 K at 10 K/min in argon. The curves exhibit the glass transition peaks with the same onset

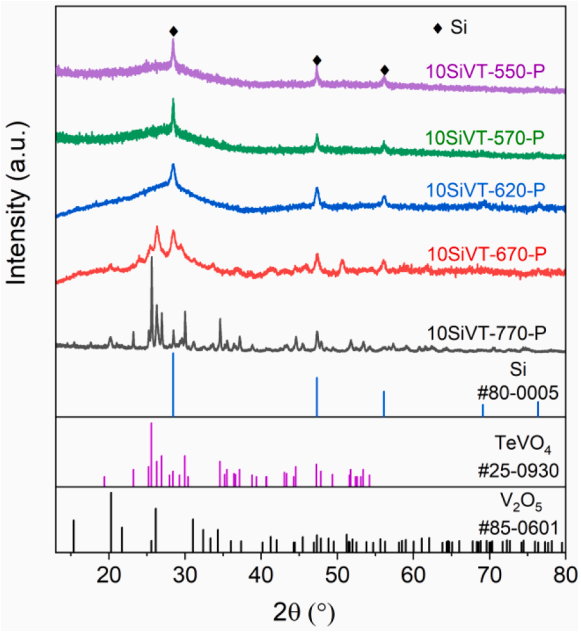

Fig. 1. XRD patterns of 10SiVT-550-P, 10SiVT-570-P, 10SiVT-620-P, 10SiVT-670-P, and 10SiVT-770-P samples, along with those of Si, $TeVO_4$ and V_2O_5 crystals.

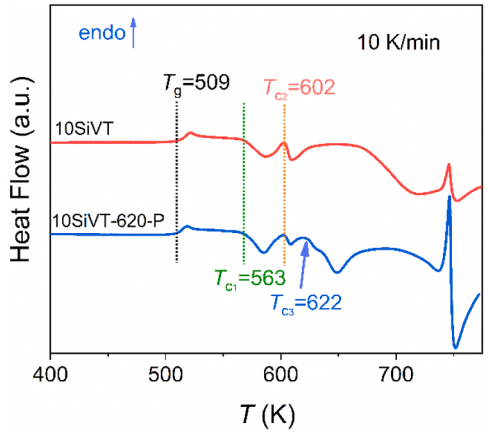

Fig. 2. DSC upscan curves of both 10SiVT (the red line) and 10SiVT-620-P (the blue line), which are obtained at 10 K/min in argon. The characteristic temperatures such as glass transition (T_g) and crystallization onset temperatures (T_{c1}, T_{c2}, and T_{c3}) are denoted in the curves.

temperature (i.e., standard glass transition temperature T_g) of 509 K, and two crystallization peaks with the same onset temperatures, i.e., T_{c1} (563 K), and T_{c2} (602 K). Interestingly, it is seen in the DSC curve of 10SiVT-620-P that a new crystallization peak emerges with an onset temperature of T_{c3}=622 K. This indicates that the hot-pressing at 620 K provides additional energy to the sample, potentially overcoming energy barrier of a redox reaction that could occur between Si and VT [16]. This reaction results in a microstructural rearrangement, facilitating the observed new crystallization event at T_{c3}. In other words, the hot-pressing process at 620 K causes different potential energy and/or structural difference between these two samples. In this context, it is more probable for 10SiVT-620-P to exhibit new crystal precipitation in the subsequent DSC scan compared to 10SiVT.

Fig. 3 shows the morphologies and EDS elemental mappings of the 10SiVT-620, 10SiVT-620-P, and 10SiVT-670-P samples, respectively. In the case of 10SiVT-620 (Fig. 3a), the SEM image and elemental mappings of Si, V, Te reveal Si nano particles agglomerating and covering the surface of VT. This observation suggests that Si is solely in physical contact with VT. Conversely, in the case of the hot-pressed samples, such as 10SiVT-620-P (Fig. 3b) and 10SiVT-670-P (Fig. 3c), there is a significant reduction in the aggregation of Si nano particles. Instead, a uniform distribution of Si within the VT glass powder is obtained. This could be attributed to two key factors. Firstly, the high temperature involved in hot pressing facilitates the diffusion of Si atoms within the mixed powder, leading to a more uniform distribution of Si. Secondly, the application of pressure during hot pressing aids in the uniform compaction of the powder, further contributing to an even distribution of Si. Additionally, the pressure plays a role in suppressing the formation of Si clusters or aggregates, thereby enhancing the bonding between Si and VT glass powder during heat treatment. Therefore, the hot-pressing method proves to be more effective in forming Si@VT composite in comparison to the heat-treatment without pressure.

To investigate the structural evolution upon heat-treatment, FTIR and XPS measurements were performed. Fig. 4 shows the FTIR spectra of Si, 10SiVT, 10SiVT-620, and 10SiVT-620-P, respectively. The peaks observed, both around 478 cm^{-1} and within the range of 1000~1250 cm^{-1} correspond to Si-O vibrations [21,22], as depicted in the spectrum of Si sample, suggesting that some of the commercial Si particles are oxidized. The intensity of the peak within the range of 1000~1250 cm^{-1} is notably higher in both the 10SiVT-620 and 10SiVT-620-P samples compared to the pristine 10SiVT, implying oxidation of Si during the heat-treatment process. It is noteworthy that, given that the heating process is conducted under vacuum conditions, only the VT glass likely acts as the oxidizing agent. The peaks at 680 cm^{-1} are ascribed to Te−O−Te or O−Te−O bonds [23], while those at around 982 cm^{-1} are attributed to [VO_5] [16,23]. It is seen that the peak at 680 cm^{-1} of 10SiVT-620-P shifted to a lower wavenumber of ~ 644 cm^{-1}. In addition, the broad peaks locating between 750 and 940 cm^{-1} are mainly due to V − O − V, [VO_4], and [VO_5] vibrations. Moreover, a shoulder at 530 cm^{-1} corresponding to V − O − V vibrations [16] was observed in 10SiVT-620 but not in 10SiVT-620-P, suggesting that the microstructural changes around V atoms is caused by applying pressure during heating process. It is worth noting that a sharp peak at 435 cm^{-1} is detected in 10SiVT-620-P which arises from Te−O−Te vibrations [24,25]. The above results imply that the microstructure around Te changes significantly by the applied pressure during heat treatment.

Fig. 5a shows the Si 2p XPS spectra for the 10SiVT, 10SiVT-620, 10SiVT-620-P, and 10SiVT-670-P samples, respectively. Each spectrum can be deconvoluted into two peaks at ~99.5 and ~103.1 eV, which are assigned to Si and SiO_2, respectively [26], as displayed in Table 1. Evidently, the ratio of Si to SiO_2 decreases with increasing the heat treatment temperature, implying that more Si is converted into SiO_2 during the heat-treatment process. In addition, the same fraction (~54.5 %) of Si in 10SiVT-620 and 10SiVT-620-P indicates that applying pressure does not facilitate the Si-to-SiO_2 conversion. The high-resolution XPS spectra of V 2p for these samples are shown in Fig. 5b. Peaks at 524.9 and 517.5 eV are ascribed to V $2p_{3/2}$ and V $2p_{1/2}$, respectively [27,28]. The V $2p_{1/2}$ peaks in the spectra of the heat-treated samples appear broader compared to that of the pristine 10SiVT sample. The broad peaks can be deconvoluted into two distinct peaks: the V^{5+} peak at 517.5 eV and V^{4+} peak at 516.4 eV [27,28]. The ratio of V^{4+} to V^{5+} increases with increasing the heating temperature, suggesting that a redox reaction occurs in 10SiVT during the heating process. Specifically, Si is oxidized by V^{5+} to form V^{4+} and SiO_2, respectively. The formation of V^{4+} could enhance the electronic conductivity in VT glass. This is because during discharging processes, polarons arise from the electron-phonon interaction, facilitating high electronic conductivity through polaron-hopping from V^{4+} to V^{5+} (V^{4+}−O − V^{5+}→V^{5+}−O − V^{4+}) [16]. However, SiO_2, another product of the redox reaction between Si and VT, lowers the electrical conductivity of the Si@VT composite materials due to its nature as an electrical insulator.

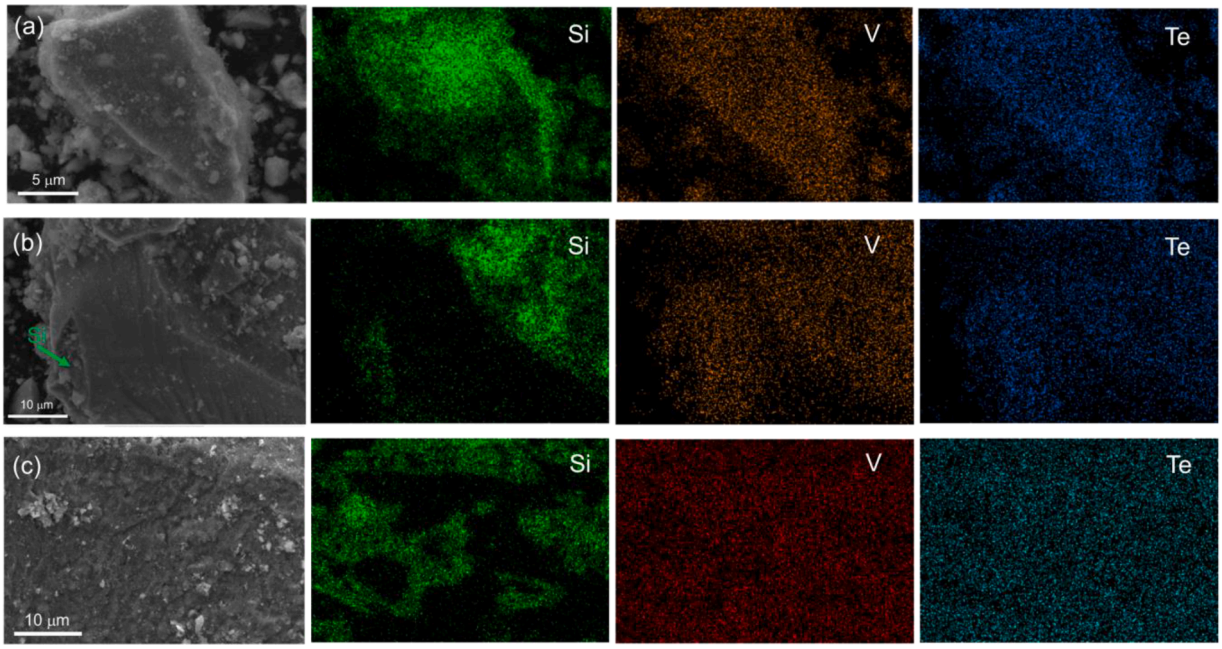

Fig. 3. SEM images and EDS elemental mappings of (a) 10SiVT-620, (b) 10SiVT-620-P, (c) 10SiVT-670-P.

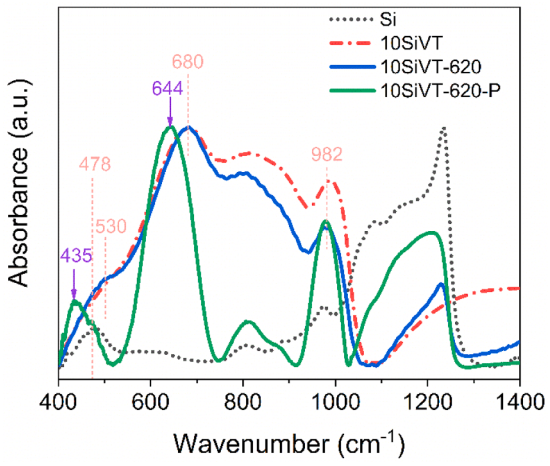

Fig. 4. FTIR spectra of Si, 10SiVT, 10SiVT-620, and 10SiVT-620-P samples.

3.2. *The ideal fabrication condition to attain a high-performance Si@VT composite anode*

To investigate the effect of both heat-treatment and hot-pressing on the electrochemical performances of the Si@VT composites in LIBs, the cycling performances of all seven composite-based anodes are compared in Fig. 6a. The Si, VT, 10SiVT-570-P, 10SiVT-620-P, 10SiVT-670-P, 10SiVT-770-P, and10SiVT-620-based anodes exhibit capacities of 28, 110, 136, 353, 274, 205, 206 mA h g^{-1}, respectively, at a current density of 1 A g^{-1} over 1000 cycles. Notably, the 10SiVT-620-P exhibits the highest capacity among them. These results imply that both the heat-treatment temperature and pressure exert a synergistic effect on the performance of the Si@VT composite based anode for LIBs. Raising heat-treatment temperature enhances the capacity of the derived anodes. However, subjecting the Si@VT composite to temperatures exceeding 620 K may lead to the formation of other crystals, such as V_2O_5 and $TeVO_4$, which do not contribute to enhancing the capacity of the composite-based anode.

The rate performances of the above-mentioned samples at the

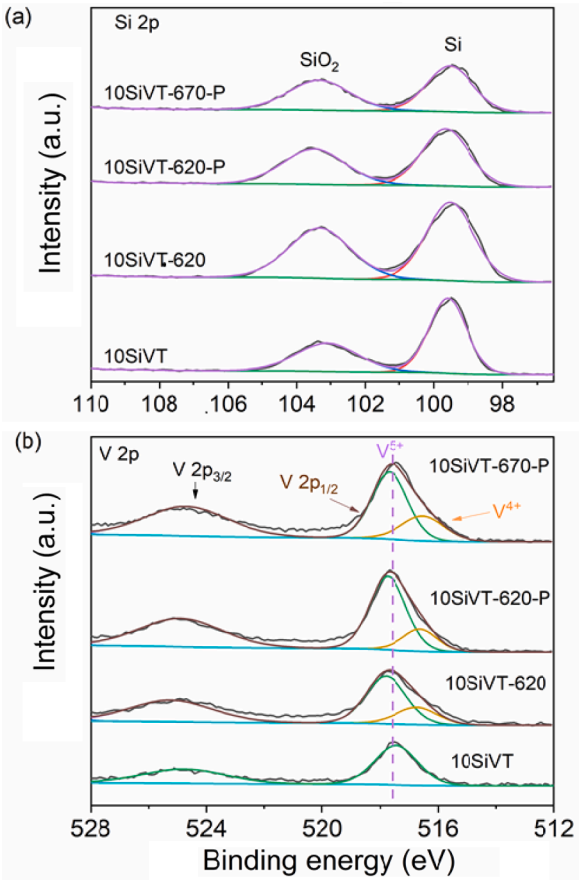

Fig. 5. XPS survey spectra and high-resolution core level of Si 2p (a) and V 2p (b) for the 10SiVT, 10SiVT-620, 10SiVT-620-P, and 10SiVT-670-P samples, respectively. The heat treatment duration: 0.5 h.

current densities of 0.1, 0.2, 0.5, 1, and 2 A g^{-1} are shown in Figs. 6b. The capacity of Si drops dramatically from 2290 to 774 mA h g^{-1} after 5 cycles, while capacities of 10SiVT-570-P, 10SiVT-620, and 10SiVT-770-

Table 1
The fractions of Si and SiO_2 in 10SiVT, 10SiVT-620, 10SiVT-620-P and 10SiVT-670-P, respectively, which were obtained from the deconvoluted Si 2p XPS spectra shown in Fig. 5a.

Samples	Si(%)	SiO_2(%)	Ratio (Si/SiO_2)
10SiVT	61.1	38.9	1.6
10SiVT-620	54.5	45.5	1.2
10SiVT-620-P	54.6	45.4	1.2
10SiVT-670-P	52.2	47.8	1.1

P decrease from ~450 to ~200 mA h g^{-1} at 0.1 A g^{-1}. Remarkably, the 10SiVT-620-P and 10SiVT-670-P based anodes exhibit the average charging/discharging capacities of 725 and 621 mA h g^{-1} after 5 cycles at 0.1 A g^{-1}, respectively. The average capacities of all the derived anodes decrease with a stepwise increase in the current density. Among the derived anodes, 10SiVT-620-P exhibits the highest capacity retention after 5 cycles at 0.2 0.5, 1, and 2 A g^{-1}. When the current density was set back to 0.1 A g^{-1}, the capacity of 10SiVT-620-P recovers to 710 mA h g^{-1} and remains stable in the following 75 cycles, indicating a superior rate performance. In contrast, the capacity of Si reaches 568 mA h g^{-1} when the current density was switched back to 0.1 A g^{-1} but decreases rapidly to 67 mA h g^{-1} after 100 cycles. This significant capacity decay of Si is attributed to its volume expansion and pulverization during cycling [29]. The higher rate capacity of 10SiVT-620-P, compared with pure Si and other samples, further supports the idea that the optimal temperature for hot pressing treatment is 620 K.

To study the impact of Si content on the electrochemical performances of the VT glass anode, we incrementally increase the Si fraction to 20 %, 30 %, and 40 %. Subsequently, a pressure of 100 MPa is applied to these mixtures by utilizing the same hot-pressing condition as applied to sample 10SiVT-620-P. The as-prepared samples are referred to as 20SiVT-620-P, 30SiVT-620-P, 40SiVT-620-P, respectively. The superior cycling performances of 10SiVT-620-P, 20SiVT-620-P, 30SiVT-620-P, 40SiVT-620-P samples are shown in Fig. 6c. Strikingly, 10SiVT-620-P sample exhibits the highest capacity of 353 mA h g^{-1} at 1 A g^{-1} after 1000 cycles.

Fig. 6d exhibits the rate performances of 10SiVT-620-P, 20SiVT-620-P, 30SiVT-620-P, and 40SiVT-620-P, respectively. In the first 5 cycles, the average capacities of the latter three samples are 808, 857, and 910 mA h g^{-1}, respectively, which are higher than that of 10SiVT-620-P (725 mA h g^{-1}). However, the capacities of these three samples are sensitive to the current density, displaying a rapid decline as the current density increases. When the current density was set back to 0.1 A g^{-1}, the capacities of the three samples are 636, 695, and 720 mA h g^{-1}, respectively, and decrease to 316, 281, and 189 mA h g^{-1} after 100 cycles. 10SiVT-620-P exhibits the capacity of 710 mA h g^{-1}, staying at 721 mA h g^{-1} even after 100 cycles, which is significantly higher compared to the other three samples. It is seen in Fig. 6 that the optimum conditions for preparing the high-performance composite is 10 wt% Si and the heat-treatment temperature of 620 K.

To confirm the optimum fraction (10 %) of Si in composite, and further to clarify the electrochemical reactions during discharging/charging cycles, Cyclic Voltammetry (CV) measurements of 10SiVT-620-P and 30SiVT-620-P were performed (Fig. 7). In the first lithiation process of 10SiVT-620-P (Fig. 7a), the reduction peaks appear at around 1.01, 0.66, and 0.02 V, which are attributed to the interaction between Li^+ and VT, formation of solid electrolyte interface film (SEI), and the insertion of Li^+ into Si forming Li_xSi phase, respectively [14,30]. The anodic peaks at around 0.34 and 0.54 V are ascribed to the extraction of Li^+ from Li_xSi, while the peaks at ~1.26 and ~2.08 V arise from the

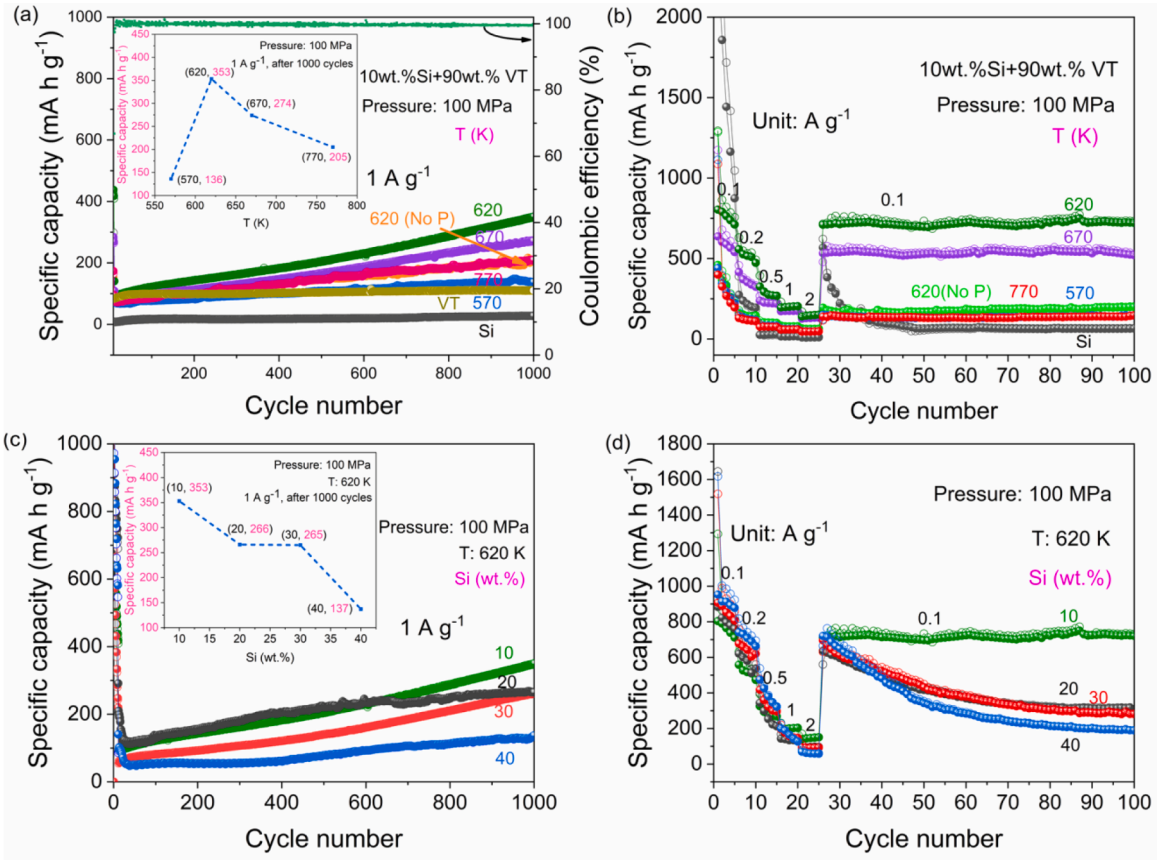

Fig. 6. Cycling and rate performances. (a), (c) Cycling performances of anodes based on Si, VT, 10SiVT-570-P, 10SiVT-620-P, 10SiVT-670-P, 10SiVT-770-P, 10SiVT-620, 20SiVT-620-P, 30SiVT-620-P, and 40SiVT-620-P at 1 A g^{-1} after 1000 cycles; (b), (d) The rate performances of anodes based on Si, 10SiVT-570-P, 10SiVT-620, 10SiVT-620-P, 10SiVT-670-P, 10SiVT-770-P, 20SiVT-620-P, 30SiVT-620-P, and 40SiVT-620-P at current densities of 0.1, 0.2, 0.5, 1, 2 and 0.1 A g^{-1}.

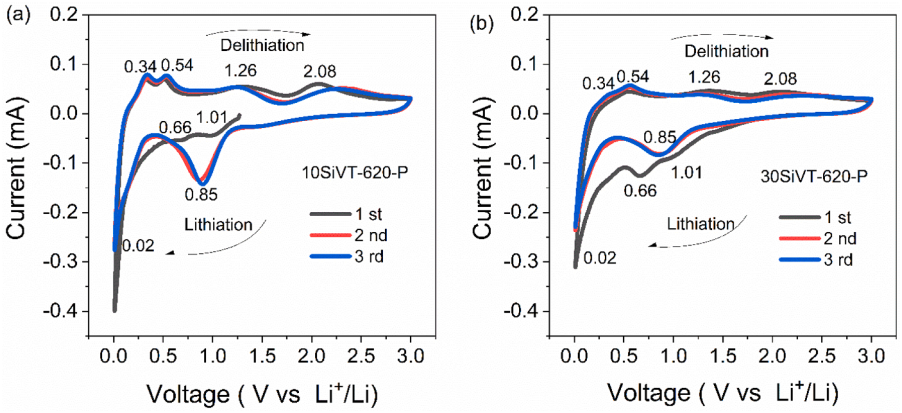

Fig. 7. Cyclic Voltammetry (CV) curves of (a) 10SiVT-620-P and (b) 30SiVT-620-P within the voltage range from 0.01 to 3.0 V at a scan rate of 0.1 mV s^{-1}.

extraction of Li^+ from VT glass matrix [14,15]. This observation implies that the incorporated Si contribute to the capacity enhancement of the composite. During the subsequent two CV cycles, peaks at 1.01 and 0.66 V disappear, being replaced by a strong peak occurs at around 0.85 V. The new peak corresponds to the insertion of Li^+ into VT glass [15].

The CV curves of the 30SiVT-620-P are shown in Fig. 7b, where the cathodic and anodic peak positions of 30SiVT-620-P are evidently identical to those observed in 10SiVT-620-P (Fig. 7a). Strikingly, each peak observed in 30SiVT-620-P appears weaker than those in 10SiVT-620-P. This implies that fewer Li^+ are inserted/extracted into/from both Si/Li_xSi and VT matrix within 30SiVT-620-P. These results suggest that even a fraction of doped Si increases, not all the Si contributes to the capacity. Once the Si particle fraction exceeds 10 % within the VT glass, the additional Si cannot be effectively integrated into the VT matrix through hot pressing. Consequently, these surplus Si particles tend to aggregate, potentially forming a SiO_2 layer on the surface of the VT particles due to oxidation of Si by the VT glass. Hence, the excess Si fails to contribute to the capacity of the Si@VT composite-based anode, leading to reductions in both capacity and cycling stability.

Fig. S2 shows the electrochemical impedance spectroscopy (EIS) of 10SiVT-620-P and 10SiVT-670-P. Each EIS curve consists of one semicircle at high frequency and an inclined line at the low frequency region. The resistance parameters (Tab. S1) are obtained from the inset equivalent circuit, where R_e, R_{ct}, C_{PE1} and Z_w represent the ohmic resistance, charge transfer resistance, interface capacitance and diffusion impedance of the half-cell systems, respectively [31,32]. The charge transfer resistance (R_{ct}) of 10SiVT-620-P (161.6 Ω) is much smaller than that of 10SiVT-670-P (354.8 Ω), indicating that the former exhibits a higher electronic conductivity, resulting in a better electrochemical performance.

The improvement in the electrochemical performance observed in Si@VT due to hot-pressing might originate from the structural synergy between the VT glass and the integrated nano-Si particles concerning the Li^+ ion storage. Fig. 8 schematically illustrated the function of VT glass matrix in suppressing the collapse of Si particles and hence in extending the cycling lifespan of Si. The detailed origin of the enhancement of Li^+ ion storage capacity in the hot-pressed Si@VT composites can be described in four aspects. 1) The disordered open network structure of VT glass is advantageous for Li^+ diffusion and storage [14,15]. 2) The VT matrix accommodates the volume expansion of nano Si particles. This buffering effect prevents their pulverization during the insertion of Li^+ into the composite, ultimately enhancing cycling stability. 3) The electronic conductivity of Si@VT can be increased by increasing V^{4+} ion content through the redox reaction between Si and VT during the heat-treatment process. 4) The pressure (100 MPa) applied by the hot-pressing process facilitates the bonding between Si and the VT glass matrix, enabling a uniform distribution of nano Si particles throughout the glass matrix. Through the above-presented experiments, we have found the following optimal fabrication conditions for obtaining the Si@VT composite exhibiting the best electrochemical performances in LIBs: 1) The Si weight fraction of 10 %; 2) The heat-treatment temperature at 620 K; 3) Hot-pressing at the pressure of 100 MPa.

4. Conclusions

A set of the Si@VT composites, comprising Si nanoparticles and vanadium-tellurite glass (VT) particles were produced through heat-treatment at different temperatures. Some of the composites were heat-treated under the isostatic pressure of 100 MPa. The composites were used as a main component of the anodes for LIBs. The Si@VT composite showed a synergistic effect, significantly enhancing its electrochemical performance. The VT glass matrix, featuring an open disordered network, not only offers voids and channels for efficient Li^+ ion storage and diffusion but also accommodates the volume changes occurring in Si throughout the discharging and charging cycles.

Our systematic characterizations of the composite-based anodes

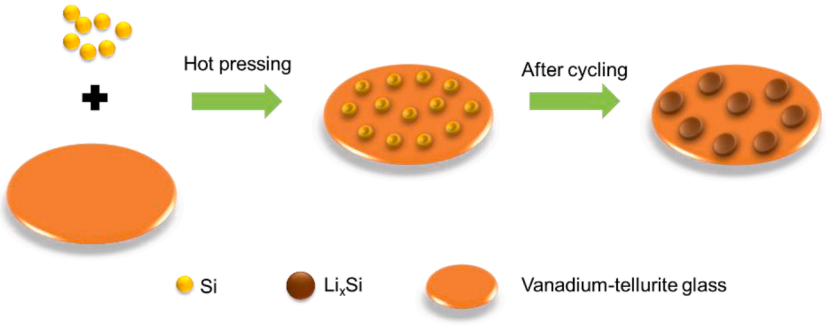

Fig. 8. The protecting role of VT glass matrix in extending the cycling lifespan of Si.

revealed the optimal conditions for fabricating the high-performance Si@VT composite: a silicon fraction of 10 wt% and a hot-pressing temperature of 620 K. The 10SiVT-620-P-based anode stood out as the optimal choice, exhibiting a capacity of 353 mA h g^{-1} at 1 A g^{-1} after 1000 cycles. This capacity surpasses that of VT glass anode by over threefold and that of pure Si anode by twelvefold.

In addition, our study revealed that the heat-treatment process under pressure facilitated the formation of V^{4+} ions through the redox reaction between Si and VT glass in the 10SiVT-620-P sample, thereby enhancing the electron transfer, and hence, increasing the electronic conductivity. The approach of fabricating Si@VT-based composite anodes holds promise for application in other suitable glass systems, potentially combined with highly active materials like SnO_2 and Sn, to further advance the development of LIBs.

CRediT authorship contribution statement

Jiajia Yan: Writing – original draft, Methodology, Data curation, Conceptualization, Investigation. **Kai Zheng:** Data curation. **Nian Shi:** Investigation, Data curation. **Xianglong Ren:** Data curation. **Hemin Zhou:** Data curation. **Haizheng Tao:** Conceptualization, Supervision. **Jinjun Ren:** Conceptualization, Supervision. **Ang Qiao:** Conceptualization. **Yanfei Zhang:** Writing – review & editing, Validation, Conceptualization, Supervision. **Yuanzheng Yue:** Writing – review & editing, Validation, Supervision, Conceptualization.

Declaration of competing interest

The authors declare that they have no known competing financial interests or personal relationships that could have appeared to influence the work reported in this paper.

Data availability

Data will be made available on request.

Acknowledgments

Authors would like to acknowledge support by China Scholarship Council (201906650022). Y.F.Z. would like to acknowledge support by Taishan Youth Scholar Project of Shandong Province (tsqn202103098), the Colleges and Universities New Twenty Terms Foundation of Jinan City (No. 202333073) and the Shandong Provincial Natural Science Foundation (ZR2020ME025).

Supplementary materials

Supplementary material associated with this article can be found, in the online version, at doi:10.1016/j.jnoncrysol.2024.122964.

References

[1] Z.H. Liu, Q. Yu, Y.L. Zhao, R.H. He, M. Xu, S.H. Feng, S.D. Li, L. Zhou, L.Q. Mai, Silicon oxides: a promising family of anode materials for lithium-ion batteries, Chem. Soc. Rev. 48 (1) (2019) 285–309, https://doi.org/10.1039/c8cs00441b.
[2] W. Hou, X. Guo, X. Shen, K. Amine, H. Yu, J. Lu, Solid electrolytes and interfaces in all-solid-state sodium batteries: progress and perspective, Nano Energy 52 (2018) 279–291, https://doi.org/10.1016/j.nanoen.2018.07.036.
[3] J. Souquet, Glasses as electrolytes and electrode materials in lithium batteries, J. Power Sources 26 (1–2) (1989) 33–35, https://doi.org/10.1016/0378-7753(89)80012-6.
[4] R. Chen, W. Qu, X. Guo, L. Li, F. Wu, The pursuit of solid-state electrolytes for lithium batteries: from comprehensive insight to emerging horizons, Mater. Horiz. 3 (6) (2016) 487–516, https://doi.org/10.1039/c6mh00218h.
[5] K. Kaup, J.D. Bazak, S.H. Vajargah, X. Wu, J. Kulisch, G.R. Goward, L.F. Nazar, A lithium oxythioborosilicate solid electrolyte glass with superionic conductivity, Adv. Energy Mater. 10 (8) (2020) 1902783, https://doi.org/10.1002/aenm.201902783.
[6] D.H.S. Tan, Y.T. Chen, H. Yang, W. Bao, B. Sreenarayanan, J.M. Doux, W. Li, B. Lu, S.Y. Ham, B. Sayahpour, J. Scharf, E. A.Wu, G. Deysher, H.E. Han, H.J. Hah, H. Jeong, J.B. Lee, Z. Chen, Y.S. Meng, Carbon-free high-loading silicon anodes enabled by sulfide solid electrolytes, Science 373 (2021) 1494–1499, https://doi.org/10.1126/science.abg7217.
[7] Y. Zhang, J. Ren, T. Xu, A. Feng, K. Hu, N. Yu, Y. Xia, Y. Zhu, Z. Huang, G. Wu, Covalent bonding of Si nanoparticles on graphite nanosheets as anodes for lithium-ion batteries using diazonium chemistry, Nanomaterials 9 (12) (2019) 1741, https://doi.org/10.3390/nano9121741.
[8] Y. Xu, Y. Zhu, C. Wang, Mesoporous carbon/silicon composite anodes with enhanced performance for lithium-ion batteries, J. Mater. Chem. A 2 (25) (2014) 9751–9757, https://doi.org/10.1039/C4TA01691B.
[9] J. Liu, P. Kopold, P.A. van Aken, J. Maier, Y. Yu, Energy storage materials from nature through nanotechnology: a sustainable route from reed plants to a silicon anode for lithium-ion batteries, Angew. Chem. 127 (33) (2015) 9768–9772, https://doi.org/10.1002/ange.201503150.
[10] X. Li, M. Zhang, S. Yuan, C. Lu, Research progress of silicon/carbon anode materials for lithium-ion batteries: structure design and synthesis method, ChemElectroChem 7 (21) (2020) 4289–4302, https://doi.org/10.1002/celc.202001060.
[11] W. Zhang, J. Li, P. Guan, C. Lv, C. Yang, N. Han, X. Wang, G. Song, Z. Peng, One-pot sol-gel synthesis of Si/C yolk-shell anodes for high performance lithium-ion batteries, J. Alloys Compd. 835 (2020) 155135, https://doi.org/10.1016/j.jallcom.2020.155135.
[12] Z. Hou, X. Zhang, J. Liang, X. Lia, X. Yan, Y. Zhu, Y. Qian, Synchronously synthesized Si@ C composites through solvothermal oxidation of Mg_2Si as lithium ion battery anode, RSC Adv 5 (87) (2015) 71355–71359, https://doi.org/10.1039/C5RA13155C.
[13] J.J. Yan, C.W. Gao, S.B. Qi, Z.J. Jiang, L.R. Jensen, H.B. Zhan, Y.F. Zhang, Y.Z. Yue, Encapsulation of nano-Si into MOF glass to enhance lithium-ion battery anode performances, Nano Energy 103 (2022) 107779, https://doi.org/10.1016/j.nanoen.2022.107779.
[14] Y. Zhang, P. Wang, T. Zheng, D. Li, G. Li, Y. Yue, Enhancing Li-ion battery anode performances via disorder/order engineering, Nano Energy 49 (2018) 596–602, https://doi.org/10.1016/j.nanoen.2018.05.018.
[15] Y.F. Zhang, P.X. Wang, G.D. Li, J.H. Fan, C.W. Gao, Z.Y. Wang, Y.Z. Yue, Clarifying the charging induced nucleation in glass anode of Li-ion batteries and its enhanced performances, Nano Energy 57 (2019) 592–599, https://doi.org/10.1016/j.nanoen.2018.12.088.
[16] J. Yan, T. Zhao, N. Shi, H. Zhan, J. Ren, Y. Zhang, Y. Yue, Impact of silicon doping on the structure and crystallization of a vanadium-tellurite glass, J. Non-Cryst. Solids 589 (2022) 121651, https://doi.org/10.1016/j.jnoncrysol.2022.121651.
[17] J. Kjeldsen, Y. Yue, C.B. Bragatto, A.C. Rodrigues, Electronic conductivity of vanadium-tellurite glass-ceramics, J. Non-Cryst. Solids 378 (2013) 196–200, https://doi.org/10.1016/j.jnoncrysol.2013.07.011.
[18] J.H. Fan, Y.F. Zhang, G.D. Li, Y.Z. Yue, Tellurium nanoparticles enhanced electrochemical performances of TeO_2-V_2O_5-Al_2O_3 glass anode for lithium-ion batteries, J. Non-Cryst. Solids 521 (2019) 119491, https://doi.org/10.1016/j.jnoncrysol.2019.119491.
[19] M.G. Moustafa, M.M.S. Sanad, M.Y. Hassaan, NASICON-type lithium iron germanium phosphate glass ceramic nanocomposites as anode materials for lithium ion batteries, J. Alloy. Compd 845 (2020) 156338, https://doi.org/10.1016/j.jallcom.2020.156338.
[20] Z.J. Jiang, T.Y. Zhao, J.J. Ren, Y.F. Zhang, Y.Z. Yue, NMR evidence for the charge-discharge induced structural evolution in a Li-ion battery glass anode and its impact on the electrochemical performances, Nano Energy 80 (2021) 105589, https://doi.org/10.1016/j.nanoen.2020.105589.
[21] I. Joni, L. Nulhakim, M. Vanitha, C. Panatarani, Characteristics of crystalline silica (SiO_2) particles prepared by simple solution method using sodium silicate (Na_2SiO_3) precursor, J. Phys. 1080 (2018) 012006, https://doi.org/10.1088/1742-6596/1080/1/012006.
[22] W. Yang, W. Huang, Q. Zheng, W. Huang, Z. Chen, High efficiency preparation, structure and properties of silicon nano-crystals by induction plasma method, NanoWorld J 2 (3) (2016) 63–68, https://doi.org/10.17756/nwj.2016-032.
[23] S. Rada, E. Culea, V. Rus, M. Pica, M. Culea, The local structure of gadolinium vanado-tellurite glasses, J. Mater. Sci. 43 (10) (2008) 3713–3716, https://doi.org/10.1007/s10853-008-2601-6.
[24] C. O'Dwyer, V. Lavayen, S.B. Newcomb, M.A. Santa Ana, E. Benavente, G. Gonzalez, C.S. Torres, Vanadate conformation variations in vanadium pentoxide nanostructures, J. Electrochem. Soc. 154 (8) (2007) K29–K35, https://doi.org/10.1149/1.2746556.
[25] M.D. Kaya, B.C. Sertel, N.A. Sonmez, M. Cakmak, S. Ozcelik, Thickness-dependent physical properties of sputtered V_2O_5 films and Ti/V_2O_5/n-Si Schottky barrier diode, Appl. Phys. A 126 (11) (2020) 1–11, https://doi.org/10.1007/s00339-020-04023-1.
[26] D.S. Jensen, S.S. Kanyal, N. Madaan, M.A. Vail, A.E. Dadson, M.H. Engelhard, M. R. Linford, Silicon (100)/SiO_2 by XPS, Surf. Sci. Spectra 20 (1) (2013) 36–42, https://doi.org/10.1116/11.20121101.
[27] G. Silversmit, D. Depla, H. Poelman, G.B. Marin, R. De Gryse, An XPS study on the surface reduction of V_2O_5 (0 0 1) induced by Ar^+ ion bombardment, Surf. Sci. 600 (17) (2006) 3512–3517, https://doi.org/10.1016/j.susc.2006.07.006.
[28] M. Taha, S. Walia, T. Ahmed, D. Headland, W. Withayachumnankul, S. Sriram, M. Bhaskaran, Insulator–metal transition in substrate-independent VO_2 thin film for phase-change devices, Sci Rep 7 (1) (2017) 1–10, https://doi.org/10.1038/s41598-017-17937-3.

[29] Y. Xu, Y. Zhu, C. Wang, Mesoporous carbon/silicon composite anodes with enhanced performance for lithium-ion batteries, J. Mater. Chem. A 2 (25) (2014) 9751–9757, https://doi.org/10.1039/c4ta01691b.
[30] S. Ashraf, R. Mehek, N. Iqbal, T. Noor, G. Ali, A. Wahab, A.A. Qayyum, A. Ahmad, ZIF 67 derived Co–Sn composites with N-doped nanoporous carbon as anode material for Li-ion batteries, Mater. Chem. Phys. 270 (2021) 124824, https://doi.org/10.1016/j.matchemphys.2021.124824.
[31] C. Gao, Z. Jiang, S. Qi, P. Wang, L.R. Jensen, M. Johansen, C.K. Christensen, Y. Zhang, D.B. Ravnsbæk, Y. Yue, Metal-organic framework glass anode with an exceptional cycling-induced capacity enhancement for lithium-ion batteries, Adv. Mater. 34 (10) (2022) 2110048, https://doi.org/10.1002/adma.202110048.
[32] X. Hu, J. Jia, G. Wang, J. Chen, H. Zhan, Z. Wen, Reliable and general route to inverse opal structured nanohybrids of carbon-confined transition metal sulfides quantum dots for high-performance sodium storage, Adv. Energy Mater. 8 (25) (2018) 1801452, https://doi.org/10.1039/C6MH00218H.